Region-Of-Interest Reconstruction on medical C-arms with the ATRACT Algorithm

Frank Dennerlein[a] and Andreas Maier[b]

[a]Siemens AG, Healthcare Sector, Erlangen, Germany
[b]Siemens AG, Healthcare Sector, Forchheim, Germany

ABSTRACT

Between 2006 and 2008, the business volume of the top 20 orthopedic manufacturers increased by 30 % to about \$35 Billion. Similar growth rates could be observed in the market of neurological devices, which went up in 2009 by 10.9 % to a volume of \$2.2 Billion in the US and by 7.0 % to 500 Million in Europe.* These remarkable increases are closely connected to the fact that nowadays, many medical procedures, such as implantations in osteosynthesis or the placement of stents in neuroradiology can be performed using minimally-invasive approaches. Such approaches require elaborate interoperative imaging technology. C-arm based tomographic X-ray region-of-interest (ROI) tomography can deliver suitable imaging guidance in these circumstances: it can offer 3D information in desired patient regions at reasonably low X-ray dose. Tomographic ROI reconstruction, however, is in general challenging since projection images might be severely truncated. Recently, a novel, truncation-robust algorithm (ATRACT) has been suggested for 3D C-arm ROI imaging. In this paper, we report for the first time on the performance of ATRACT for reconstruction from real, angiographic C-arm data. Our results indicate that the resulting ROI image quality is suitable for intraoperative imaging. We observe only little differences to the images from a non-truncated acquisition, which would necessarily require significantly more X-ray dose.

Keywords: Tomographic Reconstruction, Cone-beam CT, Region-of-interest Imaging

1. INTRODUCTION

Nowadays, many procedures in neuroradiology and surgery are performed using minimally-invasive techniques that require intraoperative imaging for guidance and quality control. This imaging task is usually covered by two-dimensional (2D) X-ray fluoroscopy on C-arm systems with a flat-panel detector. In fluoroscopy, the X-ray beam is often collimated closely to the region-of-interest (ROI) within the patient, primarily to lower radiation dose. The acquired projection images are then typically highly truncated, i.e., they may nicely show the implant or device, but not more remote areas or even the boundaries of the patient body.

For some clinical applications, projection-based imaging is not sufficient. In order to detect proper positioning of a surgical implant during a procedure, a 3D image of the implant ROI may be required.[1] Furthermore, interventional mirco devices, such as flow-diverters, often have low X-ray absorption and are barely visible in the 2D projections. However, they can be clearly seen in tomographic images and thus 3D C-arm CT has become more and more popular as a tool for intraoperative imaging. Since 3D scans cause a considerable amount of radiation dose of up to 2 mSv for a low-contrast scan of the head,[2] the idea of using both lateral and axial X-ray beam collimation also during a 3D scan appears attractive. In this manner, only the patient's ROI is being scanned, thus leading to a significant reduction of patient dose.[3]

Tomographic 3D ROI reconstruction from laterally truncated projection images is challenging and can result in a noticable degradation of image quality if no countermeasure agains the truncation is taken. Most practically-used reconstruction approaches thus try to estimate the missing projection data in a pre-processing step to allow good reconstruction.

In a recent paper,[4] however, a filtered-backprojection algorithm was presented that is intrinsically less sensitive to data truncation and does not involve an explicit estimation of missing data. So far, this algorithm (ATRACT)

Corresponding Author: Frank Dennerlein (e-mail: frank.dennerlein@siemens.com)

*Data from PearlDiver Technologies Inc, http://www.pearldiverinc.com and iData Research, http://www.idataresearch.net was evaluated on simulated data only. In this paper, we will investigate for the first time the performance of ATRACT on real projection data acquired with an interventional C-arm CT system.

2. 3D ROI RECONSTRUCTION

2.1 Preliminaries

Throughout this paper, we assume that cone-beam (CB) projection data is acquired in a standard C-arm geometry, which involves a short-scan circular X-ray source trajectory and flat-panel detector. This geometry will be described using the conventional notation that is briefly summarized in the caption of Fig. 1.

Formally, the problem of CB reconstruction can thus be expressed as recovering the object density function $f(\underline{x})$ with $\underline{x} = (x, y, z)$ from the acquired CB projection data $g(\lambda, u, v)$, where

$$g(\lambda, u, v) = \int_0^\infty f(\underline{a}(\lambda) + t\underline{\alpha}(\lambda, u, v))\, dt, \tag{1}$$

and where t indicates locations along the X-ray. We assume that projections are known over the angular interval $\lambda \in [\lambda_1, \lambda_2]$ with $\lambda_2 - \lambda_1 < 2\pi$ and that the detector area that receives valid X-ray signal is restricted in lateral direction to $u \in [u_1, u_2]$ and in axial direction to $v \in [v_1, v_2]$. In ROI tomography, on which we focus on, this detector area is supposed to be very small compared to the extent of the patient and the projections are thus severely truncated. The 3D region that is irradiated from every λ is called the field-of-view (FOV), and we assume that the geometrical set-up between scanner and patient is such that the ROI is completely contained in the FOV.

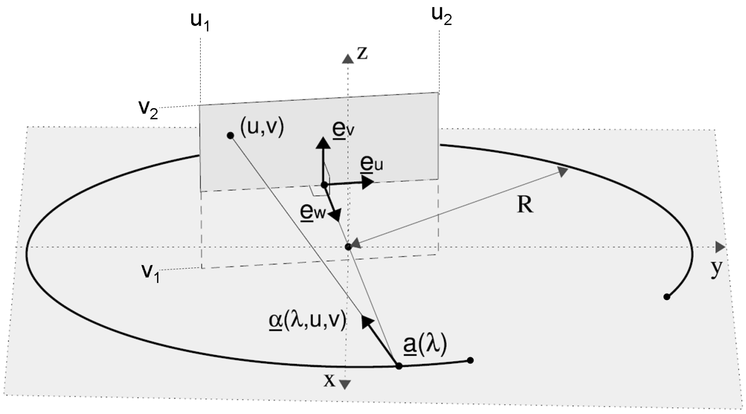

Figure 1. CB geometry and associated notation: The curve $\underline{a}(\lambda) = (R\cos\lambda, R\sin\lambda, 0)$ describes the circular trajectory of the X-ray source during the scan, with R being the scan radius and λ being the rotation angle. The planar detector is parallel to the unit vectors $\underline{e}_u(\lambda)$ and $\underline{e}_v(\lambda)$ and at distance D from the source. u and v are the coordinates, measured along those two unit vectors, that are used to describe locations of detector elements (pixels). The point $(u, v) = (0, 0)$ is attained at the orthogonal projection of the source onto the detector plane. $\underline{e}_w(\lambda)$ is the detector normal, and the unit vector $\underline{\alpha}(\lambda, u, v)$ is along the ray that connects the source at λ with the detector point (u, v).

2.2 State-of-the-art

On practical C-arm systems, the reconstruction task described above is addressed by classical filtered back projection (FBP) algorithms, with short-scan Feldkamp et al (short-scan FDK)[5] still being the most prevalent C-arm CT reconstruction approach.[6] In their original form, these algorithms come with an implicit sensitivity with respect to lateral data truncation, since they involve a 1D convolution in u with a non-local filter kernel (the ramp-filter). To carry out this convolution, and to facilitate ROI reconstruction, data extrapolation schemes were suggested to complete, in a pre-processing step, the projection data along u into the truncated area. One such method extrapolates the object contour based on mirroring of the texture at the end of the valid detector area onto a downward slope.[7] An additional multiplication with a cosine-like window function ensures a limited size of the extrapolated projection. A nice overview of this and similar methods can be found in.[8]

More recently, a reconstruction method was suggested that consists of backprojecting differentiated projection data and of iteratively deconvolving the backprojection result in the 3D image domain.[9] This method was shown to yield the correct reconstruction if a tiny bit of a-priori knowledge about f in the ROI is available.

Modifications in the acquisition strategy to reduce the difficulties of ROI imaging were described in.[10] Instead of applying real collimation, the portion of the X-ray beam that does not intersect the ROI is only attenuated using a physical X-ray filter. In this manner, a good reduction of the total dose can be achieved, while the patient is still somewhat captured in his entire lateral extent. The truncation occurring in a collimated ROI scan can also be handled if a previous, non-collimated scan of the complete object is available[11] and if the data of both scans are appropriately combined prior to reconstruction. Such modifications in the acquisition mode, however, are not considered in this paper.

As another practical alternative for ROI reconstruction, we recently suggested the *approximate, truncation-robust algorithm for computed tomography* (ATRACT), in 2011.[4] This algorithm was shown to give very promising results on simulated data, but its performance on real CB data has still been unclear. Main subject of the following sections is thus a further, real-data evaluation of ATRACT.

3. THE ATRACT ALGORITHM

The ATRACT method for ROI reconstruction from severely-truncated projections was originally introduced in.[4] It was derived by analytically reformulating the standard short-scan FDK algorithm[5] into a reconstruction scheme that is by construction less sensitive to lateral data truncation. Below, we describe a slight modification of that original algorithm. First, the reconstruction formulas are given, followed by an intuitive explanation of the underlying concepts. The (modified) ATRACT reconstruction is achieved using the steps:

ATRACT

1	Data weighting	$g_1(\lambda,u,v) = \dfrac{D\ m(\lambda,u)}{\sqrt{D^2+u^2+v^2}}\, g(\lambda,u,v)$
2	2D Laplace filtering	$g_2(\lambda,u,v) = \left(\dfrac{\partial^2}{\partial u^2}+\dfrac{\partial^2}{\partial v^2}\right) g_1(\lambda,u,v)$
3	2D residual filtering	$g_F(\lambda,u,v) = \int_{u_1}^{u_2}\int_{v_1}^{v_2} g_2(\lambda,u',v')h_{2D}(u-u',v-v')\,du'\,dv'$
4	3D CB backprojection	$f(\underline{x}) = \int_{\lambda_1}^{\lambda_2} \dfrac{RD}{[R-\underline{x}\cdot\underline{e}_w(\lambda)]^2}\, g_F(\lambda,u^*,v^*)\,d\lambda$

The function $m(\lambda, u)$ in step 1 is a Parker-like weighting function,[12] used to approximately handle redundancies in the short-scan data. In step 4, u^* and v^* are the coordinates of the CB projection of the point $\underline{x}$ on the detector. Note that the difference to the previously published algorithm lies in the realization of step 3, which was previously derived as the filter operation:

$$g_F(\lambda,u,v) = \frac{1}{4\pi^2}\frac{R}{D}\int_0^{\pi} |\cos\mu|\, g_3(\lambda,\mu,s^*)\,d\mu \tag{2}$$

where $s^* = u\cos\mu + v\sin\mu$ and where

$$g_3(\lambda,\mu,s) = \int_{-\infty}^{\infty} g_2(\lambda, s\cos\mu - t\sin\mu, s\sin\mu + t\cos\mu)\,dt \tag{3}$$

This filter corresponds to a 2D Radon transform, an angle-dependent weighting and a 2D backprojection; it is thus shift-invariant. Instead of an explicit implementation of (2) and (3) in the reconstruction algorithm, we

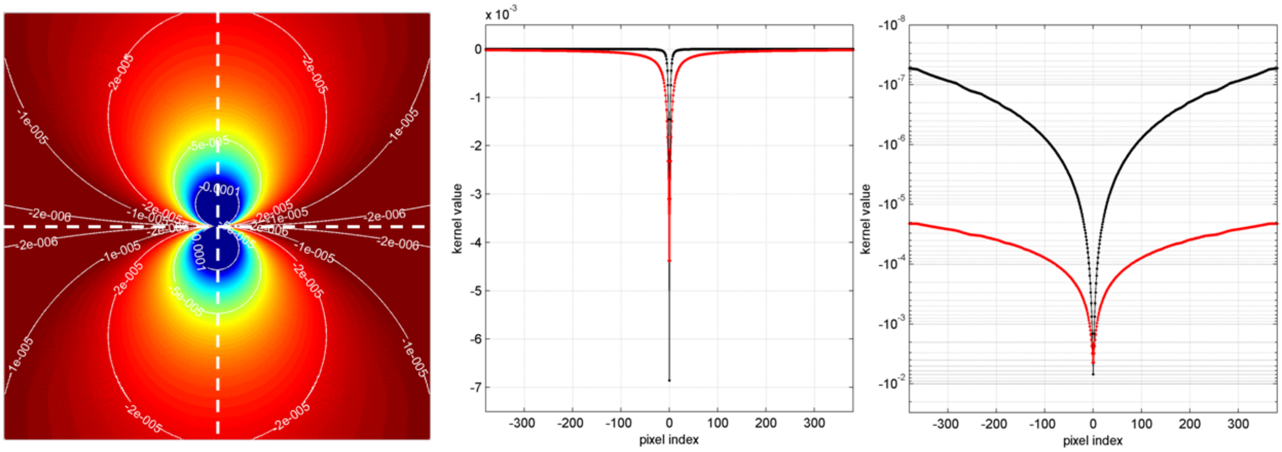

Figure 2. The filter kernel h_{2D}. (Left) Color-coded illustration of the kernel values with white curves indicating constant values. Note that red corresponds to 0, while dark blue corresponds to large negative values (colors in electronic version only). (Center) Profile of the kernel values along the dashed horizontal line, v=0, in the left figure (black) and along the dashed vertical line, u=0, in the left figure (red). (Right) The same profiles plotted in a logarithmic scale.

here first numerically compute the 2D impulse response of this filter to obtain the kernel h_{2D}, and then carry out the discrete 2D convolution described above. The resulting 2D kernel is illustrated in Fig. 2. Interestingly, this kernel decays fairly fast towards 0 along the u-axis, while its entries of higher magnitude are distributed along the v-axis; see also the profiles in the center and right of this figure. Note also that such a kernel was also found to be useful in the context of phase-contrast CT.[13]

Intuitively, the idea behind ATRACT is to adopt the general scheme of short-scan FDK, but to decompose its 1D ramp-filter operation into two successive 2D filter steps (Steps 2 and 3). The first of these filters (2D Laplace operation) acts purely locally on the projections image and can thus be carried out accurately over the valid intervals in u and v, even if projections are truncated laterally[†]. In this aspect, ATRACT significantly differs from FDK that comes with a one-step non-local 1D filtering that is - as a whole - significantly affected by this scenario of truncation. Furthermore, note that the 2D Laplace filter has also some sparsifying character, i.e., the values of g_2 are much closer distributed around 0 than the values of g_1. The implicit assumption that g_2 is constant 0 outside the known area, as will be used when restricting the bounds of integration to $u \in [u_1, u_2]$ and $v \in [v_1, v_2]$ in the 2D convolution in step 3, is thus a good approximation. Consequently, even though no explicit extrapolation scheme was involved during the filtering operation, the resulting g_F will have a low level of disturbing truncation artifacts. The results of,[4] in fact, indicate that remaining 3D artifacts are of rather low-frequency, offset-like characteristics.

4. REAL-DATA EVALUATION

4.1 Scan Configurations

We will now evaluate the performance of ATRACT for real-data ROI reconstruction on an interventional C-arm (Siemens Artis Zee system). Three scan configurations are considered. In configuration one (CFG1), no collimation was applied during the scan, yielding non-truncated projections on the entire area of the detector ($u_1 = -200mm$, $u_2 = 200mm$, $v_1 = -150mm$, $v_2 = 150mm$ on the considered system). Using the results of CFG1, the ROI in the patient was specified. For configuration two (CFG2) the projections acquired in CFG1 were virtually cropped so that for every image only the small region was kept onto which the specified ROI projects. Note that dependent on the location of the ROI, the virtual cropping for CFG2 occurs at parameters u and v that may vary from one image to the other. In configuration three (CFG3), we repositioned the object so that the ROI is centered on the C-arm rotation axis, and acquired data using a physical collimation of the X-ray

[†]Note that in the numerical implementation, one row/column at each boundary of the valid detector are is lost when implementing the Laplace operation using a 3x3 kernel.

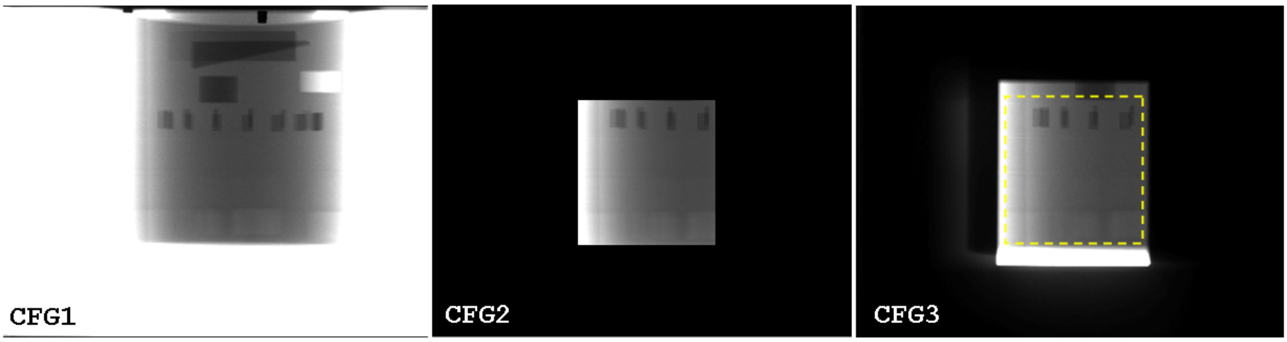

Figure 3. Sample projection image (of the CB phantom) in the considered scan configurations. (Left) CFG1 - where no collimation was used, (center) CFG2 - where the projections from CFG1 were virtually cropped so that only the projection of the ROI remains, (right) CFG3 - where physical, static collimation of the X-ray beam to a central detector area was used during the scan.

beam to a central region on the detector. This physical collimation does not vary with λ. Sample projections for all three configurations are displayed in Figs. 3 and 6.

For the presented evaluation, the short-scan FDK reconstructions of CFG1, i.e., of the non-truncated data, will be used as a benchmark. The reconstructions in CFG2 and CFG3 will be carried out using the ATRACT algorithm and will be visually and quantitatively compared to the benchmark results, after resolution matching is achieved. Since ATRACT reconstructions from truncated data may suffer from an off-set like artifact, we furthermore automatically find a global correction of scaling and bias to align the range of values between the considered algorithms. Note that the differences between CFG1 and CFG2 on one hand and CFG3 on the other hand lie in the level physical effects, such as X-ray scatter, in the projections and also in the fact that object repositioning took place between those scans. We therefore expect differences in the reconstruction results, even if the sizes of the detector area in CFG2 and CFG3, for which the data are available, are identical.

4.2 Reconstruction Results

The study presented in this section involves two real C-arm data sets. Data set 1 was obtained from a physical CB phantom, which contains several low- and high-contrast inserts useful for evaluation of image quality; see Fig. 3. Data set 2, which is displayed in Fig. 6, was acquired in a clinical environment during the placement of a neurological stent[‡].

[‡]Data courtesy of Baylor College of Medicine, Houston, TX, USA

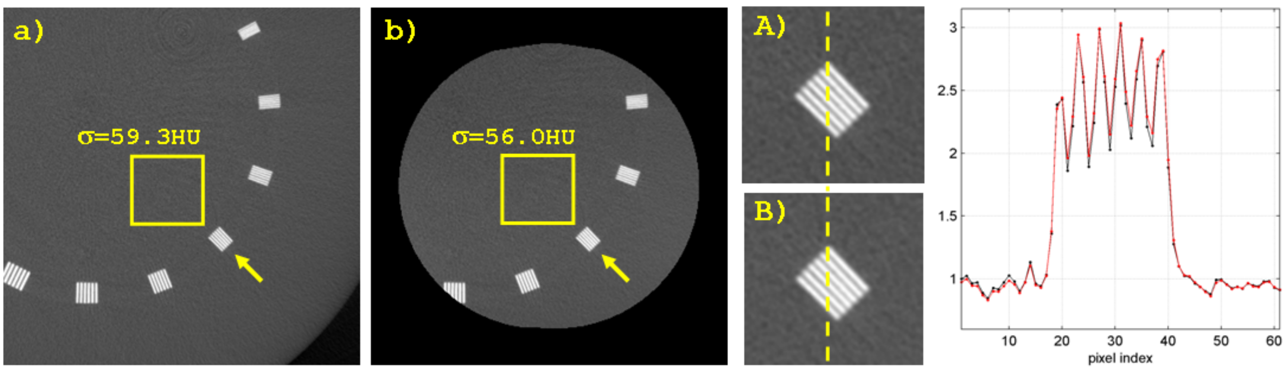

Figure 4. Reconstructions of the resolution inserts of the CB phantom in the grayscale window [-1000 HU,2000 HU] and using isotropic voxels of size 0.25mm. a) Short-scan FDK reconstruction in CFG1 (zoom of the insert indicated with an arrow is shown in A), b) ATRACT reconstruction in CFG2 (zoom given in B). The profiles through the investigated insert along the vertical, dashed line are given on the right; almost no difference can be seen. In the left two slices, we furthermore display the noise level for the yellow rectangular region.

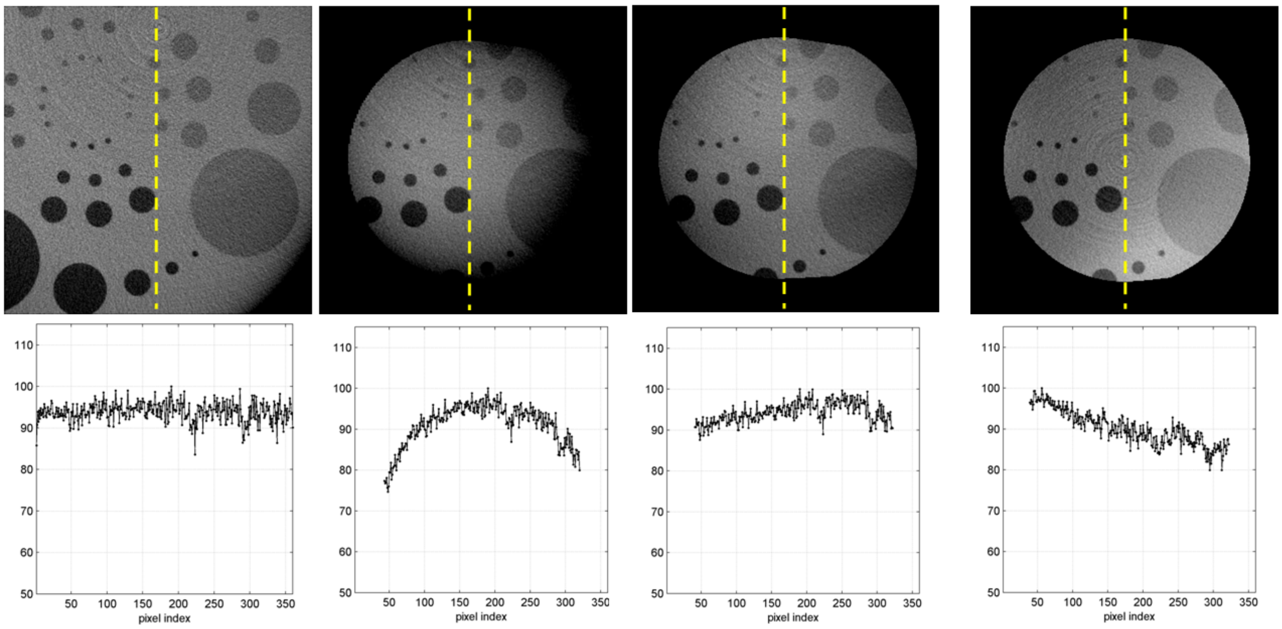

Figure 5. Reconstructions of the low-contrast inserts of the CB phantom in the narrow grayscale window [-250 HU,150 HU], using voxels of size 0.25mm and a slice thickness of 3.5 mm. From left to right: Short-scan FDK reconstruction in CFG1, Short-scan FDK with constant data extrapolation in CFG2, ATRACT reconstruction in CFG2, ATRACT in CFG3. The second row shows the values along the profiles indicated with a dashed line.

Fig. 4 shows, for CFG1 and CFG2, the reconstructions of some radially aligned line-pair inserts of the CB phantom, together with profiles through one of these inserts. These results confirm that our algorithmic implementations of ATRACT and short-scan FDK yield essentially same spatial resolution. The image noise, estimated by calculating the standard deviation over a central rectangular area in the presented slices, are also not significantly different (59.3 HU vs. 56.0 HU).

Other parts of the CB phantom contain low-contrast inserts that are here used to assess truncation artifacts. Corresponding slices are displayed in Fig. 5, using a compressed grayscale window to emphasize image gradients. To appreciate the effctive suppression of radial truncation artifacts by the ATRACT method, the results of short-scan FDK with constant explicit row-wise data extrapolation are displayed (in CFG2). As can be seen, this extrapolation cannot completely avoid the radial gradient-like truncation artifacts. A better result in CFG2 is obtained by ATRACT that yields a reconstruction close to the benchmark. The results from CFG3 also avoids the radial artifact, but comes with a small linear gradient, which turned out to be caused by the proximity of

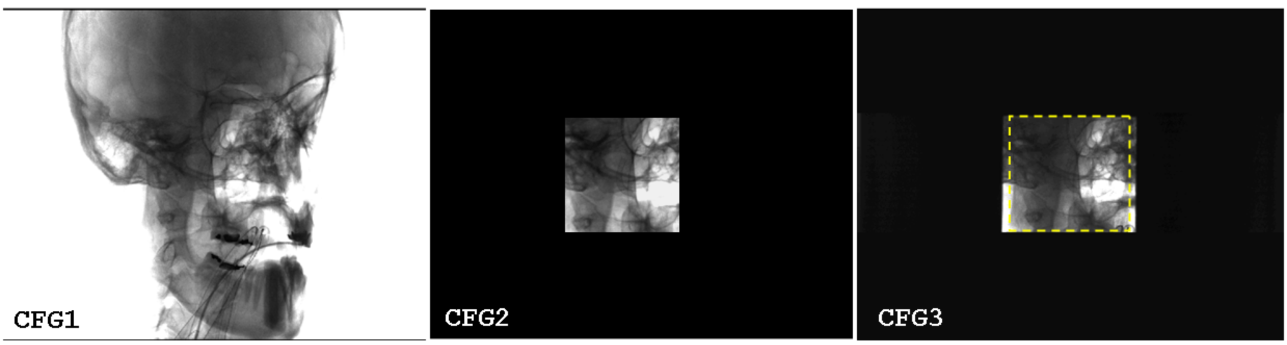

Figure 6. A projection image of the clinical head patient data set. (Left) CFG1 - full detector, (center) CFG2 - virtual cropping, (right) CFG3 - physical collimation (the yellow rectangle shows the data not affected by the shadow of the collimator and thus used for reconstruction).

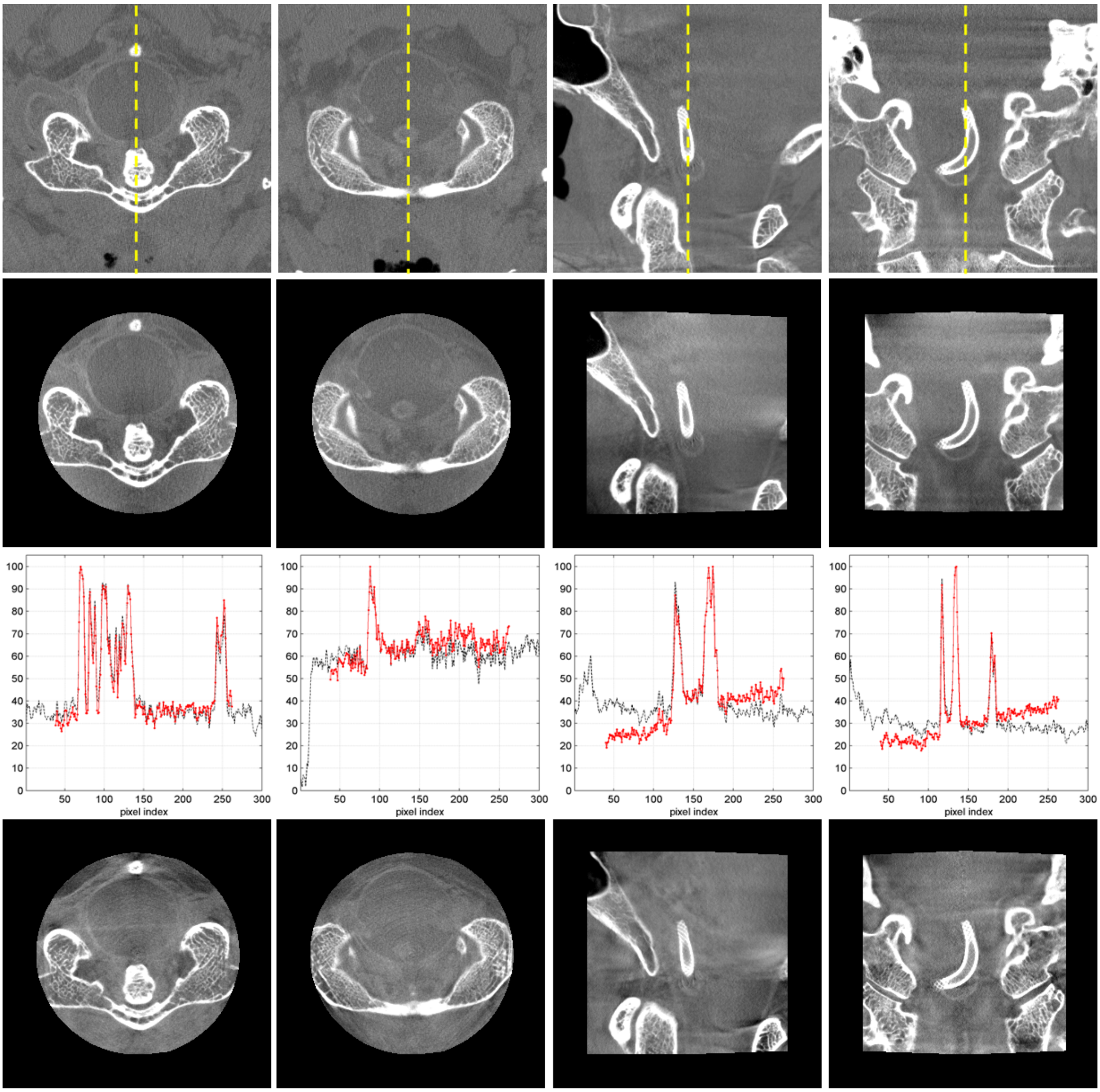

Figure 7. Slices through the ATRACT results of the clinical data set, in the grayscale window [-800 HU,2200 HU]. From left to right: two transversal slices of thickness 0.75 mm, one sagital slice and one coronal slice, each of thickness 1.5 mm. The top row shows the reconstructions obtained from the non-collimated scan (CFG1) and row 2 the corresponding slices from the virtually cropped data set (CFG2). The reconstructed values (after normalization) along the central profiles indicated as a dashed-yellow line are given in row 3. At the bottom, the corresponding slices obtained from the collimated scan (CFG3) are given. The regions outside the field-of-view are indicated in black.

the slice to the edge of axial truncation.

The reconstructions of the clinical data set are shown in FIG. 7. All configurations are displayed together, and additional profiles through some slices are given to quantitatively compare the results of CFG1 and CFG2. From these profiles, we notice that ATRACT yields very good image quality in axial slices, but is somewhat affected by axial data truncation; see the gradient in the rightmost images. The physical collimation yields similarly good results, but CFG3 comes with some less homogeneous background, i.e. with structural artifacts that are not observed in CFG2. We hypothesize that this degradation is caused by the projection preprocessing on the C-arm system, which was not optmized for processing data of collimated 3D scans. Overall, however, the feasibility of ATRACT for clinical ROI C-arm CT is demonstrated.

5. CONCLUSIONS

Previous reports on the ATRACT algorithm only presented successful reconstructions on numerical phantom data. It is well known that the application to real data is often much more difficult. As can be seen in the results from the previous section, however, the ATRACT method provides visually very satisfying reconstructions from real data, even in presence of severe data truncation. The algorithm thus turns out to be robust with respect to physical effects occuring during C-arm acquisition, such as polychromatic or scatter effects. In terms on noise and spatial resolution, no significant differences to short-scan FDK were observed. Confirming the simulation results published in,[4] gradient-like truncation artifacts are effectively reduced in strength. The ATRACT results, however, contain some slight, remaining low-frequency artifacts, compared to the benchmark results, and these artifacts appear to be strongest close to the bottom and top the FOV. We again notice that the values reconstructed with ATRACT suffer from a global scaling and bias. This effect, however, can be accounted for by adapting the visualization parameters, or by applying a global scaling and bias to the final volume. Future work might cover finding projection preprocessing parameters that optimize image quality for the ROI application.

Acknowledgements

The autors would like to thank G. Kleinszig for discussions and input about clinical applications of ROI imaging in surgery. The concepts and information presented in this paper are based on research and are not commercially available.

REFERENCES

[1] K. Wendl, B. Vock, J. von Recum, P. A. Gruetzner, and A. Wentzensen. *Trauma und Berufskrankheit: 8 Jahre Erfahrung mit intra-operativer 3D-Bildgebung (German)*. Springer, 2009.

[2] N. Strobel, O. Meissner, J. Boese, T. Brunner, B. Heigl, M. Hoheisel, G. Lauritsch, M. Nagel, M. Pfister, E.-P. Rhrnschopf, B. Scholz, B. Schreiber, M. Spahn, M. Zellerhoff, and K. Klingenbeck-Regn. Imaging with flat-detector c-arm systems. In *Multislice CT*, pages 33–51. Springer, 2009.

[3] S. H. Fung, Y. Chang, R. Pino, E. S. Hui, X. Zhou, M. V. Alvarado, G. Benndorf, O. M. Diaz, R. P. Klucznik, Z. Xiong, S. T. Wong, and K. C. Li. Dynamically collimated c-arm flat panel detector ct imaging for focussed region-of-interest reconstruction and radiation dose reduction. In *Proc. ASNR 2011*, page no pagination. ASNR, 2011.

[4] F. Dennerlein. Cone-beam roi reconstruction using the laplace operator. In *Proc. Fully 3D 2011*, pages 80–83. Institute of Medical Physics, University of Erlangen-Nuremberg, 2011.

[5] L. A. Feldkamp, L. C. Davis, and J. W. Kress. Practical cone beam algorithm. *Optical Society of America*, 1:612–619, 1984.

[6] A. C. Kak and M. Slaney. *Principles of Computerized Tomographic Imaging*. IEEE Service Center, Piscataway, NJ, United States, 1988.

[7] B. Ohnesorge, T. Flohr, K. Schwarz, J. P. Heiken, and K. T. Bae. Efficient correction for CT image artifacts caused by objects extending outside the scan field of view. *Medical Physics*, 27:39–46, 2000.

[8] G. Van Gompel. *Towards accurate image reconstruction from truncated X-ray CT projections*. University Antwerpen, Antwerpen, Belgium, 2009.

[9] H. Kudo, M. Courdurier, F. Noo, and M. Defrise. Tiny a priori knowledge solves the interior problem in computed tomography. *Physics in Medicine and Biology*, 53:2207–2231, 2008.

[10] R. Chityala, K. R. Hoffmann, D.R. Bednarek, and S. Rudin. Region of Interest (ROI) Computed Tomography. *Proc Soc Photo Opt Instrum Eng*, 5368(2):1018–4732, 2004.

[11] D. Kolditz, Y. Kyriakou, and W. A. Kalender. Volume-of-interest (VOI) imaging in C-arm flat-detector CT for high image quality at reduced dose. *Medical Physics*, 37(6):2719–2730, 2010.

[12] D. L. Parker. Optimal short scan convolution reconstruction for fanbeam CT. *MP*, 9(2):254–257, 1982.

[13] A. V. Bronnikov. Phase-contrast ct: Fundamental theorem and fast image reconstruction algorithms. In *Proc. SPIE*, page 63180Q, 2006.